Chapter-IV

Double Perovskite Sr_2NiMoO_6 Based Anode Systems

Paper published from this chapter

1. Pravin Kumar, *Nitish Kumar Singh and Prabhakar Singh*, Influence of Ni/Mo ratio on structural and electrical properties of double perovskite system* $Sr_2Ni_{1+x}Mo_{1-x}O_{6-\delta}$*, Appl. Phys. A (2014).*

2. Pravin Kumar, *Rajesh Kumar Singh[1]and Prabhakar Singh[1]*, Structural and electrical behavior of double perovskite material* $Sr_2NiMoO_{6-\delta}$*, Advanced Science Letters, Vol. 20, 647–649, (2014).*

4.1 Overview

In the development of SOFCs, perovskite and double perovskite materials are technologically important due to their applications in the fields of renewable energy **[**Cowin et al. (2011), Huang, et al. (2006) and Wang et al. (2011)]. Perovskites are materials having ABO_3 formula unit with ideal cubic structure, where A is an alkaline earth or rare earth cation (Ca, Sr, La etc.), and B is an electronically active transition metal cation (Mn, Fe, Co, Ni, V, Cu etc.). The double perovskite with general formula $A_2B'B''O_6$ follows the layered structure of perovskite ABO_3, where A is an alkaline earth element (A = Sr, Ca, Ba) while and B′, B″ are heterovalent transition metals (B′ = Fe, Cr, Fe, Co, Ni, etc. and B″ = Mo, W, Re, Sb, etc.) [Poddar et al. (2004), Chenet et al. (2005), Lufaso et al. (2006), Kong et al. (2009), Marrero-Lo´pez, et al. (2010), Vasala et al. (2011), Aguadero et al. (2011), and Troncoso, et al. (2013)]. The double perovskites $A_2B'B''O_6$ represent two types of octahedral viz $B'O_6$ and $B''O_6$, oriented in three dimensions of crystal lattice [Dorai et al. (2013) and Prasatkhetragarn et al. (2009)]. Among such kinds, molybdenum based double perovskites exhibit exceptional electromechanical properties. Many of them are highly enviable in SOFC for their superior performance as anode materials [Huang, et al. (2006), Graves et al.(2010) and Wei et al. (2000)]. Due to these reasons, some of these materials having mixed electronic and ionic conductions (MEICs) such as $Sr_2MgMoO_{6-\delta}$ [Marrero-Lo´pez, et al. (2010), Vasala et al. (2011)], Sr_2CoMoO_6 [Aguadero et al. (2011)], $Sr_2FeMoO_{6-\delta}$ [Wang et al. (2011)], and $Sr_2NiMoO_{6-\delta}$ [Lufaso et al. (2006), Wei et al.(2000)] have been studied at large-scale for their high electrical conductivity and good catalytic activity under different reducing atmospheres (air/H_2/H_2-Ar/CH_4). Among them, $Sr_2NiMoO_{6-\delta}$ is a potential candidate for anode material in SOFC. However, functionality of $Sr_2NiMoO_{6-\delta}$ faces severe challenges due to the formation of secondary phases, which leads generally owing to inadequate heat treatments [Graves et al.(2010)]. Prasatkhetragarn et al.[2009] reported that an extra addition of NiO (5 wt. %) in Sr_2NiMoO_6 system eliminates the secondary phase of $SrMoO_4$ [Prasatkhetragarn et al. (2009)]. In $Sr_2NiMoO_{6-\delta}$, formation of single phase occurs after heat treatment above 1200 ˚C [Prasatkhetragarn et al. (2009), and Huang, et al. (2009)]. Also, Ni doped double perovskite are important because of its high catalytic activity in comparison to Ni-free double perovskite anode materials [Xiao et al. (2011) and (2012)]. These reports motivated the researchers to investigate Ni substituted double perovskites for anode materials in SOFC. Few authors have

also reported that Sr_2NiMoO_6 exhibits a second order phase transition from tetragonal (s.g.*I4/m*) to cubic (s.g.$Fm\bar{3}m$) at temperatures around 300 ˚C [Lufaso et al. (2006)], 280 ˚C, [Prasatkhetragarn et al. (2009)] and 277 ˚C [Eriksson et al.]. XPS studies for $A_2FeMoO_{6-\delta}$ (A = Ca, Sr, Ba) systems show that the reduction of Mo^{6+} state into Mo^{5+} affects the electrical conductivity [Li et al. (2011)]. While Dorai et al. [2013] reported that in $Sr_2MgMoO_{6-\delta}$, oxygen vacancies are created due to the reduction of Mo^{6+} state to Mo^{5+}. In Sr_2MMoO_6 (M=Mg, Mn, Fe, Co, Ni and Zn) systems, Co, Ni, and Zn based systems are stable under oxidizing conditions whereas Mn and Fe based systems are stable under reducing condition simultaneously Mg based systems are found to be stable in both reducing and oxidation atmospheres [Vasala et al. (2010)]. Huang et al. [2009] investigated that the conductivity of $Sr_2NiMoO_{6-\delta}$ increases with increasing temperature and grain boundary parameters. Recently, a research group reported the enhanced electrical conductivity in molybdate based ceramic samples due to the formation of oxygen vacancies and electronic defects [Filonova et al. (2014)]. The thermal study of $Sr_2NiMoO_{6-\delta}$ represented the linear thermal expansion behaviour from room temperature to 950 ºC (average TEC value is ~ 12.14 $\times 10^{-6}$ K^{-1}) [Wei et al. (2000)]. In this chapter, the effect of the relative change of ratio Ni/Mo on the phase formation of double perovskite $Sr_2NiMoO_{6-\delta}$ has been studied. Also the structural & electrical properties are reported in detail in this chapter.

4.2 Influence of Ni/Mo Ratio on Structural and Electrical Properties of Double Perovskite System $Sr_2Ni_{1+x}Mo_{1-x}O_{6-\delta}$

In the present chapter, the system $Sr_2Ni_{1+x}Mo_{1-x}O_{6-\delta}$ ($0.00 \leq x \leq 0.15$) has been synthesized via a facile sol-gel technique. The structural, thermal, and electrical properties of above this system has been studied employing powder XRD, SEM, XPS, dilatometry and impedance spectroscopy techniques, respectively. The compositions with x = 0.00, 0.05, 0.10, and 0.15 in the system $Sr_2Ni_{1+x}Mo_{1-x}O_{6-\delta}$ (SNM-x) are prepared and designated as SNM00, SNM05, SNM10, and SNM15, respectively.

4.3 Results and Discussion

4.3.1 XRD Analysis

Phase investigation, crystal-structure and lattice parameters of the system $Sr_2Ni_{1+x}Mo_{1-x}O_{6-\delta}$ were determined by powder XRD technique. Figure 4.1(a)-(d) shows the

XRD patterns of the system $Sr_2Ni_{1+x}Mo_{1-x}O_{6-\delta}$ with $0.00 \leq x \leq 0.15$. The peak profiles of the XRD pattern exhibits a well crystalline nature of the prepared samples. The peaks corresponding to major phase could be indexed on the basis of double perovskite tetragonal phase Sr_2NiMoO_6 with space group *I4/m* using JCPDS card no. 15-0601.

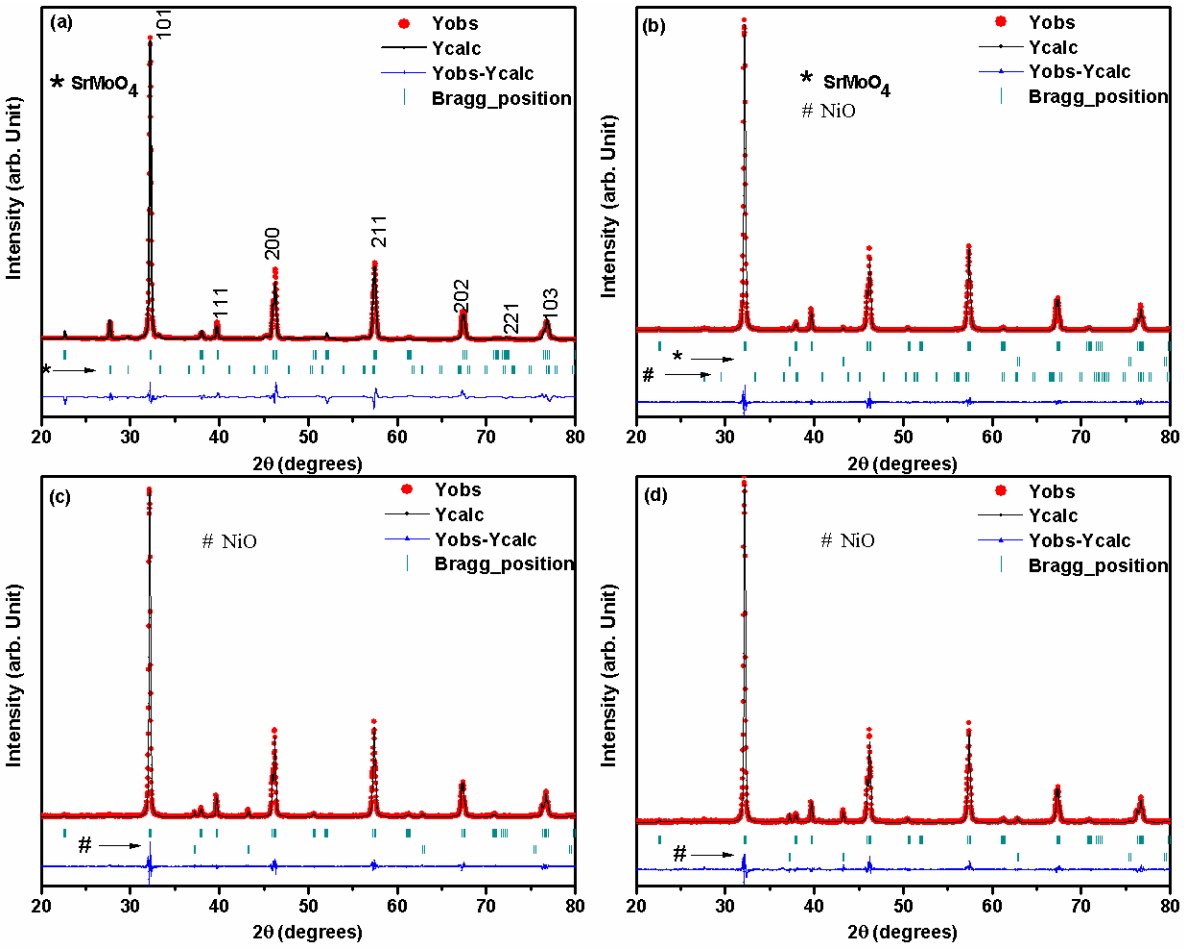

Fig. 4.1*: Rietveld refinement of X-ray diffraction pattern of various compositions* ***(a)*** *SNM00,* ***(b)*** *SNM05,* ***(c)*** *SNM10 and* ***(d)*** *SNM15. Here Yobs, Ycal, and Yobs-Ycal represent the experimental data, calculated data, and the difference of experimental and calculated data, respectively.*

In the XRD pattern of sample SNM05 two minor phases, $SrMoO_4$ and NiO, were detected whereas for sample SNM00, only one minor phase of $SrMoO_4$ and for samples SNM10 and SNM15, only one minor phase of NiO were detected. The peaks corresponding to the observed minor phases could be indexed as a $SrMoO_4$ tetragonal phase with space group $I4_1/a$ using JCPDS card no. 85-0586 and NiO Cubic phase with space group $Fm\bar{3}m$

using JCPDS card no. 04-0835. The Rietveld refined XRD patterns of all samples are also shown in Fig.4.1(a)-(d). The refinement was using *Fullprof* software and the refined parameters are mentioned in Table 4.1. In the sequential refinement channels, the peak profiles were modelled by pseudo-Voigt function by considering the six coefficient polynomial background. The R_{wp} (weighted-pattern factor) and S (goodness-of-fit) parameters are taken as numerical criterion for the quality of the fit between experimental and calculated diffraction data. The R values (R_p), weighted profile R values (R_{wp}), and χ^2 values indicate that the refinement results are admissible and consistent with the published literature. The refinement results also show that the increase of x value i.e. Ni content, on the one hand suppresses the $SrMoO_4$ phase but on the other hand creates the NiO phase.

Table 4.1.*Various parameters obtained from Rietveld refinement of XRD data of the SNM-x system ($0.00 \leq x \leq 0.15$).*

Parameters	**SNM00**	**SNM05**	**SNM10**	**SNM15**
Lattice Parameters	a = b = 5.5406 c = 7.8786	a = b = 5.5498 c = 7.8931	a = b = 5.5494 c = 7.8914	a = b = 5.5499 c = 7.8922
Unit cell volume	241.863	243.119	243.026	243.093
R_p	19.1	11.2	12.3	13.2
R_{wp}	17.8	15.5	16.8	18.0
χ^2	1.43	2.22	2.52	3.01

Lattice parameters of the system SNM-x determined by XRD patterns using Rietveld refinement is shown in Fig.4.2. It can be seen that lattice parameters increase rapidly for SNM05 and afterward approximately constant for SNM10 and SNM15. The increase in the lattice parameters for SNM05 may be due to the combined effect of two reasons, first one is substitution of greater ionic radii of dopant ions Ni^{2+} (0.69Å) at the place of the smaller ionic radii of host ions Mo^{6+} (0.59 Å) [Shannon et al. (1976)] and second one is creation of oxygen vacancies on substitution of Ni on Mo site [Wei et al. (2012)].

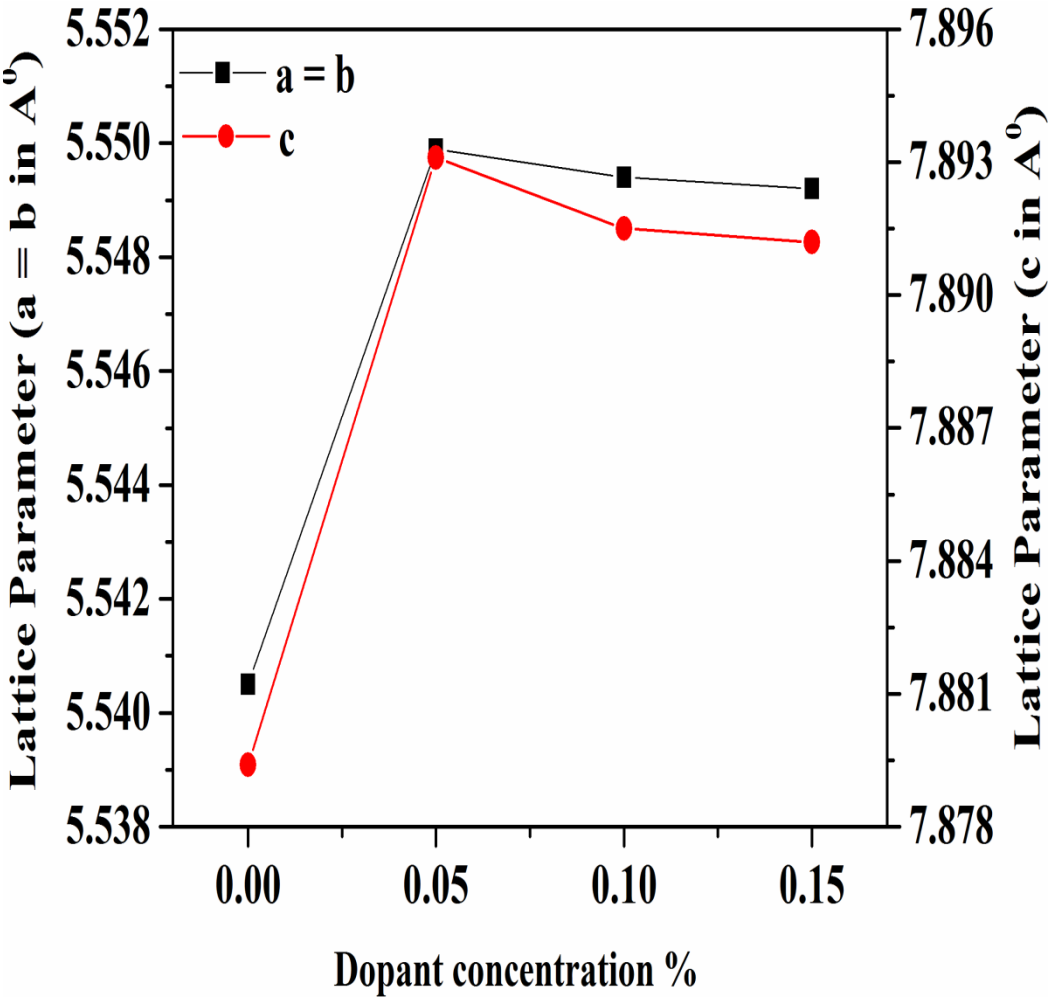

Fig. 4.2: *Variation in lattice parameters as a function of the dopant concentration for the system SNM-x (0.00 ≤ x ≤ 0.15).*

4.3.2 Microstructure Study

The microstructures of the chemically etched samples of the system SNM-x are shown in Fig.4.3 (a)-(d). From microstructure, it can be clearly seen that the sample SNM00 has larger grain size as compared to other samples. It is decreased for x=0.05 but the further increment of Ni ions increases the size of grains in gradual manner. This behaviour can be seen numerically by determining the size of the grains for each composition using linear intercept method and it were found to be approximately ~3.35 μm, ~1.5 μm, ~1.68 μm and ~1.81 μm for compositions SNM00, SNM05, SNM10, and SNM15, respectively.

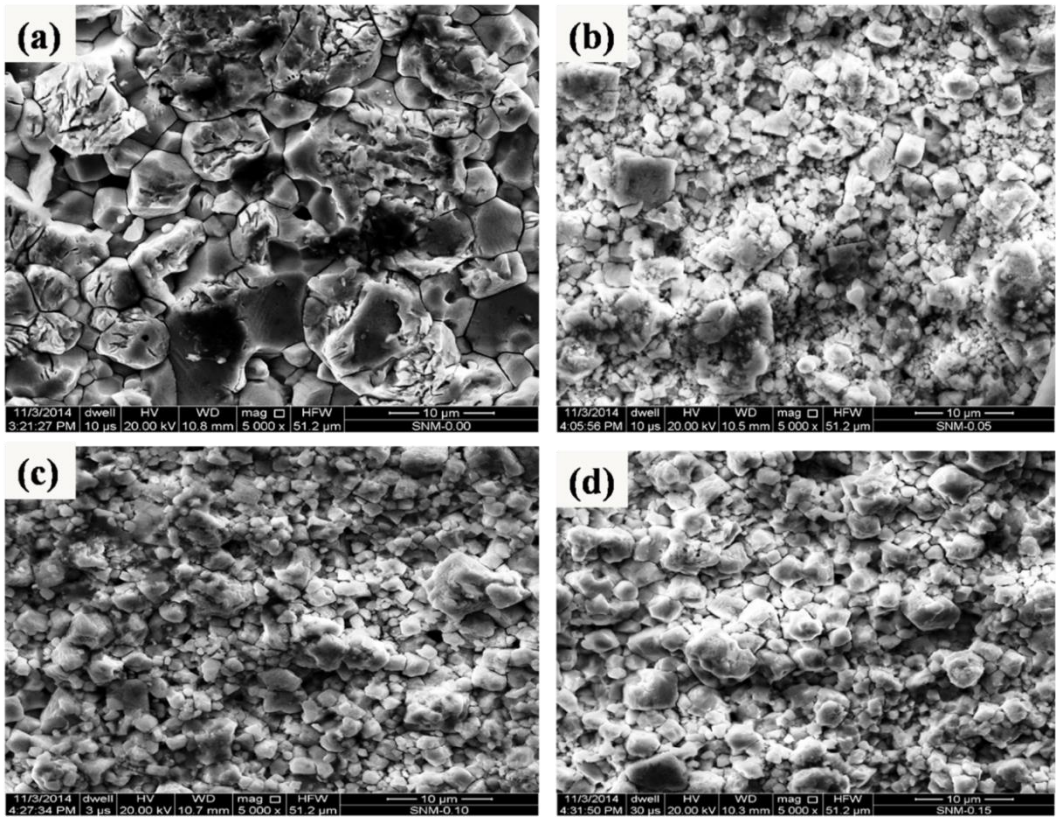

Fig. 4.3: *Field emission scanning electron micrograph of chemically etched various compositions (a) SNM00, (b) SNM05, (c) SNM10 and (d) SNM15.*

4.3.3 TEC Study

Thermal Expansion Coefficient is one of the important parameters for the materials used as a component in SOFCs. Because, to prolong the life of cells, the compability of cell components should be thermally compatible. The variation in thermal expansion coefficient (TEC) with temperature for all the prepared compositions of the system SNM-x is shown in Fig. 4.4. From evident, it reveals the non-linear behaviours below 100 ˚C and linear behaviour above it. It is also clear that the slope of the samples SNM00, SNM05 and SNM10 is stepper than that of the slope of the sample SNM15. This indicates that the sample SNM15 is more thermally stable than the other samples. Also, increased thermal stability was observed with increasing Ni content. The average TEC value for all the compositions was calculated from the slope of the curve. In the calculation, linear region was considered. The average value of TEC for all the compositions are mentioned in Table 4.2. These values are lower than the value reported earlier in literature for samples $Sr_2Ni_{0.75}Mg_{0.25}MoO_6$ (12.3-13.5×10^{-6} K^{-1}) **[**Filonova et al.(2014)] and Sr_2NiMoO_6 (12.14×10^{-6} K^{-1}) [Wei et al. (2000)]. The low values

of TEC for these samples are well matched with the standard electrolyte materials $Zr_{0.84}Y_{0.16}O_{1.92}$ (11×10^{-6} K^{-1}) and LSGM ($10\text{-}13\times10^{-6}$ K^{-1}) [Zajac et al. (2007) and Tietz et al. (1999)]. Therefore, these samples will provide better thermal compatibility as compared to the commonly used electrolytes.

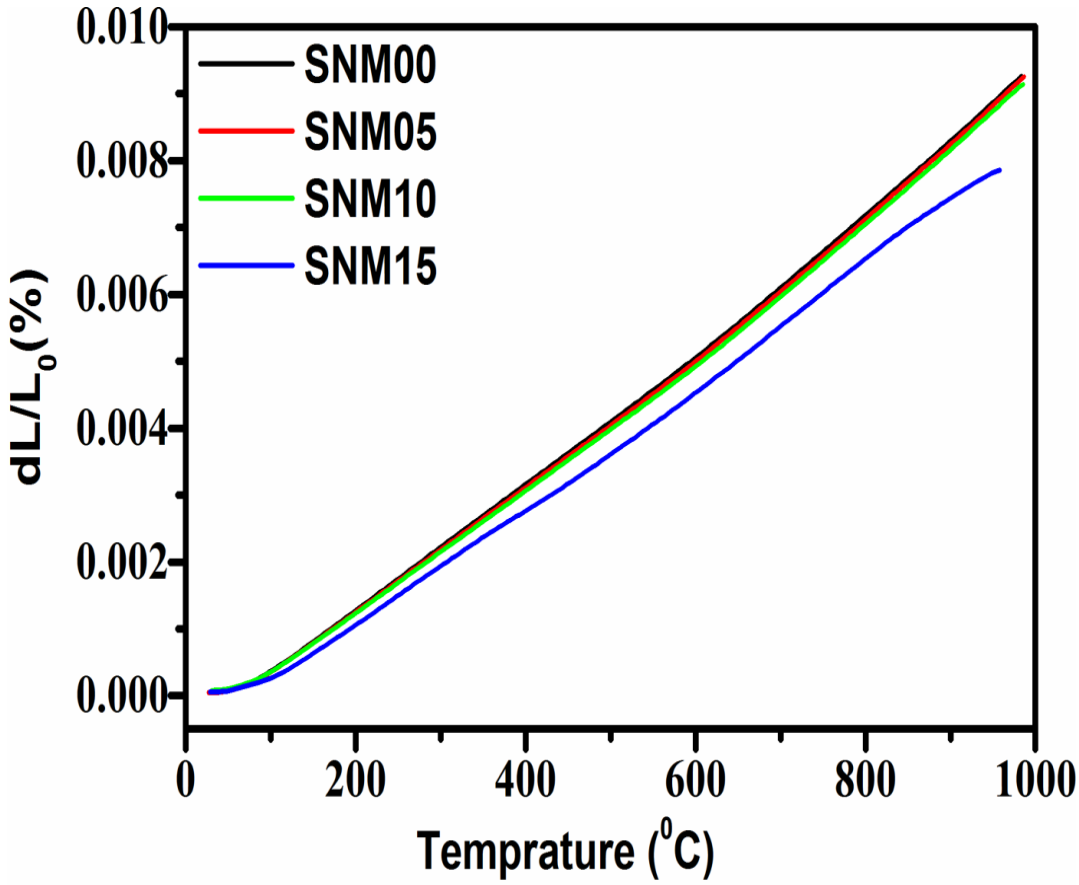

Fig. 4.4: *The variation of average TEC value for compositions SNM00, SNM05, SNM10 and SNM15.*

Table 4.2: *The Variation of average TEC value of SNM-x (x=0.00, 0.05, 0.10, and 0.15) system.*

Compositions	Average TEC value (K^{-1})
SNM00	9.8×10^{-6}
SNM05	9.8×10^{-6}
SNM10	9.7×10^{-6}
SNM15	8.9×10^{-6}

4.3.4 XPS Analysis

To confirm the oxidation state of the different elements present in the prepared samples, XPS measurement was carried out. The obtained XPS spectrums corresponding to Sr, Ni, Mo and O for the system SNM-x are schematically shown in Fig.4.5 (a)-(d). The obtained XPS spectra were corrected with respect to C 1s peak appeared at ~284.6 eV. From Figure 4.5 (a), it can be seen that the Sr-3d core level spectra has asymmetrical peak for all the samples. This peak could be de-convoluted into two peaks corresponding to $3d_{5/2}$ (~133 eV) & $3d_{3/2}$ (~135 eV) corroborating the presence of Sr^{2+}. The Ni-2p XPS spectra for SNM00 show two peaks at ~855.7 eV and ~874.1 eV which are assigned to Ni^{2+} $2P_{3/2}$ and $2P_{1/2}$, respectively. This indicates that most of the Ni in sample SNM00 is bivalent. For other samples, these peaks shift towards lower energy, implying an increase of Ni^{3+} content in the samples. The Mo-3d XPS spectra shown in Fig.4.5 (c) are splitted into two asymmetrical peaks; these peaks could be designated to $3d_{5/2}$ and $3d_{3/2}$ states. These peaks could be fitted to two pairs of peaks which could be assigned to Mo^{5+} and Mo^{6+} states [Dambies et al. (2001)]. The details of binding energy for all the samples are listed in Table 4.3.

Table 4.3. *Fitting results of Mo-3d XPS spectra and percentage of adsorbed oxygen of the system SNM-x ($0.00 \leq x \leq 0.15$).*

Compositions	Parameters	Mo^{6+}		Mo^{5+}		Mo^{6+}/Mo^{5+}	Adsorbed oxygen %
		$3d_{5/2}$	$3d_{3/2}$	$3d_{5/2}$	$3d_{3/2}$		
SNM00	Binding Energy(eV)	234.74	238.02	234.07	237.75	0.92	23.85
	Area	6978.43	4673.93	5429.78	7214.63		
SNM05	Binding Energy(eV)	233.88	237.31	233.23	236.64	1.56	34.93
	Area	11156	5766.49	5081.58	5766.91		
SNM10	Binding Energy(eV)	233.05	237.83	232.35	235.83	1.83	15
	Area	1674.08	4149.05	1651.10	1528.67		
SNM15	Binding Energy(eV)	233.83	236.99	231.85	236.58	2.74	10.65
	Area	6116.80	2953.32	357.11	2953.32		

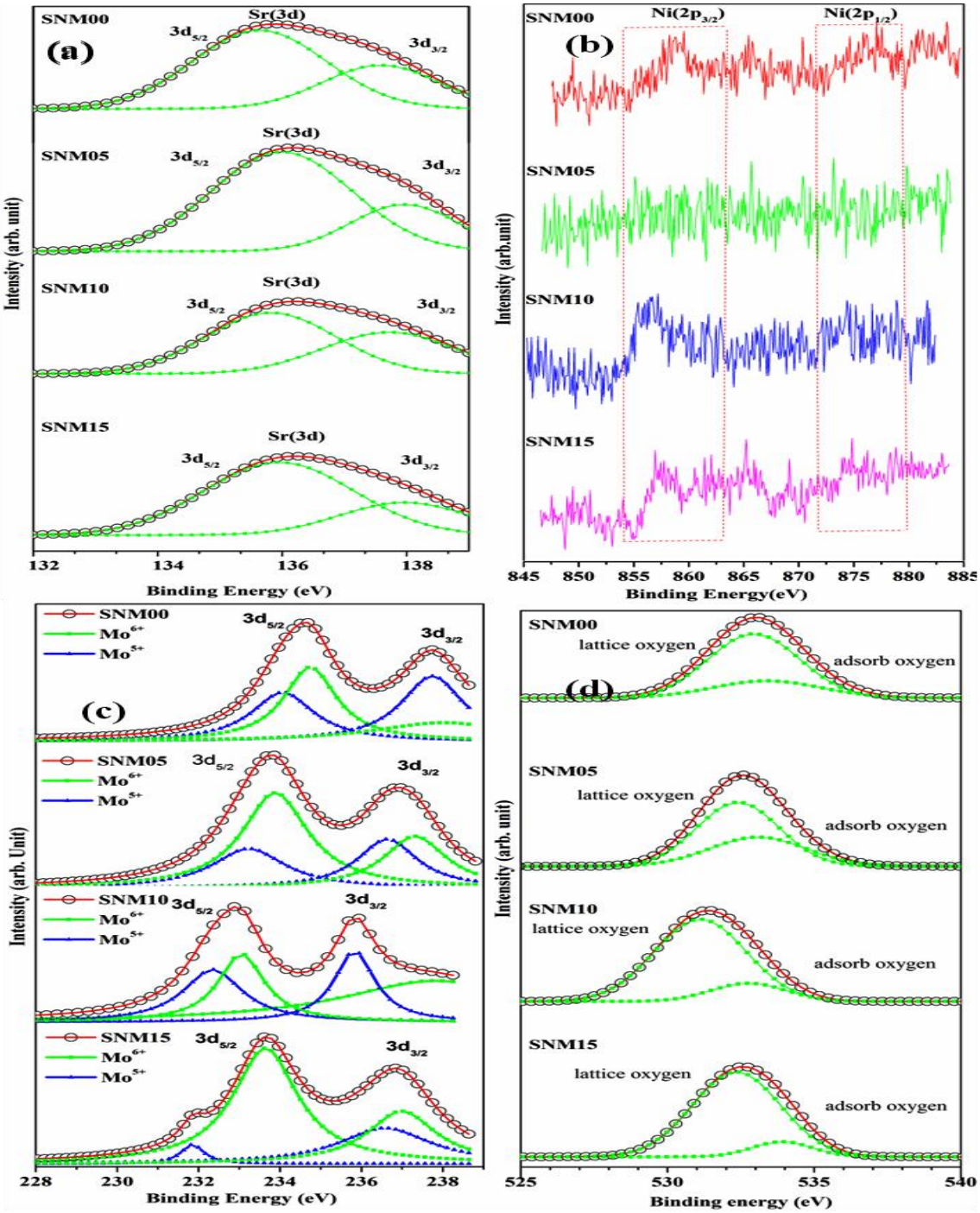

Fig.4.5: *XPS spectra for compositions SNM00, SNM05, SNM10 and SNM15: (a) Sr-3d, (b) Ni-2p, (c) Mo-3d and (d) O-1s.*

Although, all the samples exhibit mixed valance state of Mo^{5+}/Mo^{6+}, but Ni substitution for Mo, increases the ratio of Mo^{6+}/Mo^{5+} with increasing Ni content, which was determined by the ratio of the integrated areas of Mo^{6+} and Mo^{5+} peaks. Figure 4.5 (d) shows O-1s core-level

spectrum which is asymmetrical in nature for all the samples. These peaks could be de-convoluted into two peaks. These peaks correspond to two different kinds of oxygen species: lattice oxygen and adsorbed oxygen. The percentages of adsorbed oxygen are shown in Table 4.3. This indicates that on Ni substitution the percentage of adsorbed oxygen increases for sample SNM05 and on further Ni substitution the percentage of adsorbed oxygen decreases. Thus the composition SNM05 has better catalytic activity towards the oxygen association/dissociation process [Xie et al. (2014)].

4.3.5 Electrical conductivity

Impedance spectroscopy is a prominent tool for analyzing the electrical transport property of materials and the electrochemical reactions at interfaces [Macdonald et al. (1987)]. An impedance spectrum is represented by Nyquist plot. This consists of three semi-circular arcs corresponding to grains, grain-boundaries and electrode interface polarization in the sequence of decreasing frequency, respectively. Each contribution can be modelled by parallel combination of resistance and capacitance. But in practical materials, generally depressed semi-circular arc is obtained due to distribution of relaxations [Hodge et al. (1976)]. Thus in practical materials each contribution is modelled by parallel combination of resistance and constant phase element [Macdonald et al. (1987)]. In the impedance spectra of the present system, two depressed semi-circular arc were observed in the entire measured frequency range. The first semi-circular arc in the high frequency range corresponds to grains contribution while second one in the low frequency range corresponds to grain-boundaries contribution. The complex plane impedance plots for sample SNM05 at a few temperatures are shown in Fig.4.6 (a)-(f) as a representative for studied system. It is clear from above figure that on increasing temperature, the arcs corresponding to each contribution shifted towards the higher frequency due to decrease in relaxation time of the corresponding polarization. Thus at higher temperature the arcs corresponding to grain- boundary was only seen with the evolution of arc corresponding to electrode polarization. This nature of appearance is a consequence of the limited frequency range available for measurement. If long span of frequency range were available the arc corresponding to each three contribution would have been appeared.

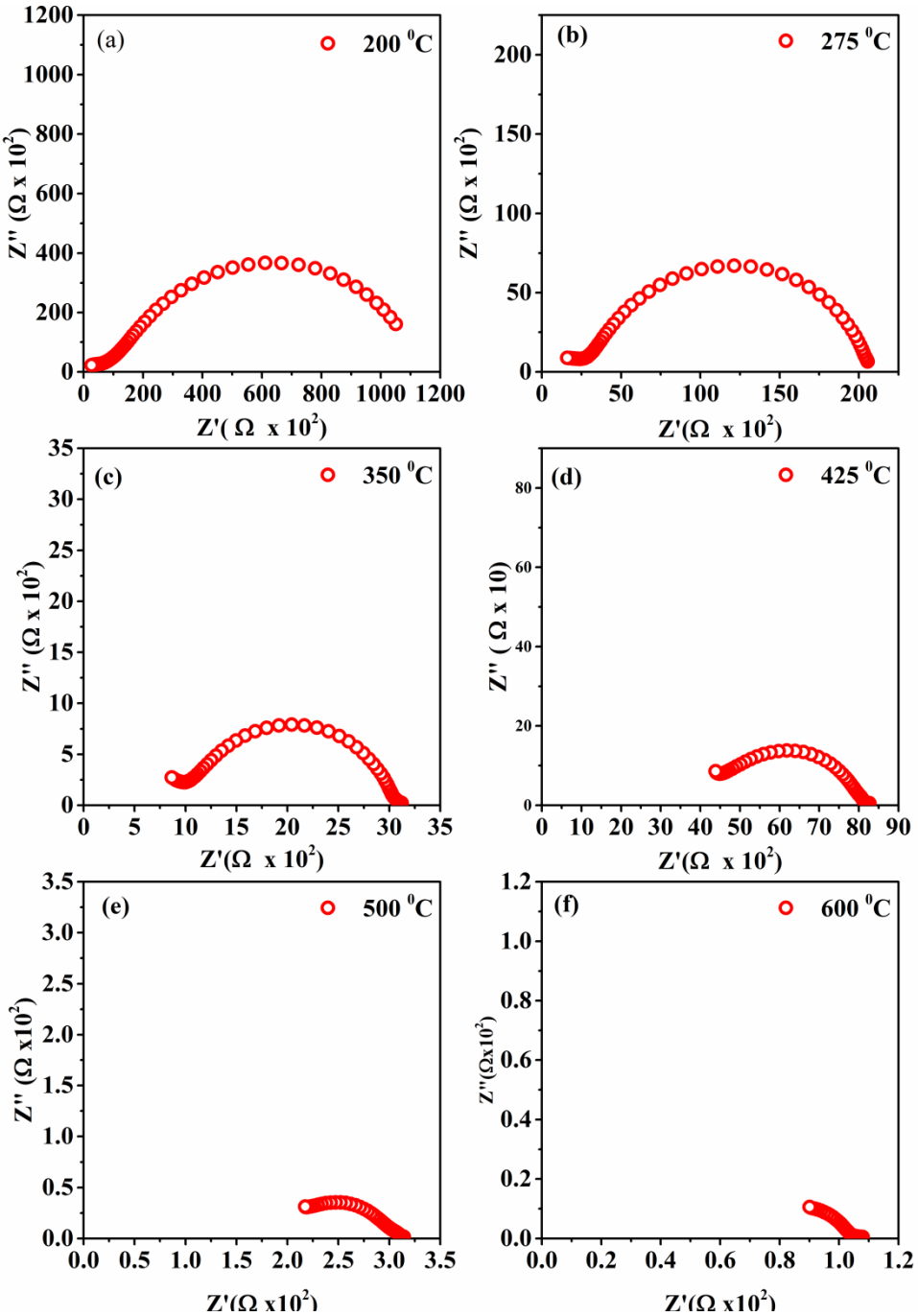

Fig. 4.6: *The complex plane Impedance plots for the composition SNM05 at* ***(a)*** *200 ˚C,* ***(b)*** *275 ˚C,* ***(c)*** *350 ˚C,* ***(d)*** *425 ˚C,* ***(e)*** *500 ˚C and* ***(f)*** *600 ˚C.*

The complex plane impedance plots at 250 °C for all the prepared compositions are shown in Fig. 4.7(a)-(d) to study the variation of impedance with dopant concentration. From the figure, it can be observed that with increase in Ni content, the total impedance for sample SNM05 decreases significantly as compared to sample SNM00 but further increment of Ni content increases the total impedance of samples SNM10 and SNM15 gradually. Also, it is

worthwhile to notice that the increment of Ni content increases the contribution of grain-boundaries impedance to the total impedance. The variation of impedance is directly related to the conduction behaviour of the system, which has been explained in the forthcoming paragraphs. The intercept of a particular semi-circular arc with the real axis represents the resistance of that particular contribution. Hence the depressed semi-circular arc corresponding to grains provides grain resistance, R_g while the semi-circular arc corresponding to grain-boundaries gives grain-boundary resistance, R_{gb}. Therefore, the total resistance, R_t , of the sample is determined by

$$R_t = R_g + R_{gb} \tag{4.1}$$

The total conductivity, σ_t of the samples can be calculated using the formula

$$\sigma_t = \frac{1}{R_t} \times \frac{t}{A} \tag{4.2}$$

where, *t* is the thickness of pellet, *A* is the area of pellet. The temperature dependence of total conductivity, determined using the equation (4.2), has been plotted on logarithmic scale with reciprocal of the absolute temperature as shown in Fig.4.8, using the relation

$$\sigma_t = \frac{\sigma_o}{T} \exp\left(-\frac{E_a}{kT}\right) \tag{4.3}$$

where σ_o is known as pre-exponential factor, E_a is the activation energy, k is the Boltzmann constant and T is the absolute temperature. It is clear from the Figure 4.8 that all samples except SNM00 showed one linear region. The sample SNM00 showed two linear regions separated by the temperature 300 °C. This is the temperature near phase transition for sample SNM00 at which it goes from tetragonal to cubic phase [Lufaso et al. (2006)]. It also evidenced that the increase of Ni/Mo ratio stabilizes the tetragonal phase as no change in slope is observed with increasing Ni/Mo ratio. The activation energy of conduction for all the compositions, obtained by the least square fitting of the data points, is given in Table 4.4.

The value of activation energy for I region of sample SNM00 indicates the domination of electronic conduction over oxide ion conduction, whereas, the value of activation energy for II-region indicates the domination of oxide ion conduction over the electronic conduction. But other all samples show values of activation energy that reflects dominant nature of electronic conduction over oxide ion conduction in the entire temperature range. This trend of activation

energy may be correlated with the structure. In region I, SNM00 possess tetragonal phase while in region II it possess cubic phase. But other samples possess stabilized tetragonal phase over the entire temperature range of measurement. Thus it can be inferred that the tetragonal phase promotes the electronic conduction whereas cubic phase promotes the oxide ion conduction because of open structure to oxide ions movement. At lower temperature sample, SNM05 has higher electronic conductivity than that of the samples SNM10 and SNM15 because of lower ration of Mo^{6+}/Mo^{5+} which will increase the carrier concentration of $\left[Mo_{Mo^{6+}}^{5+}{}'\right]$ and also the higher oxide ion conductivity due to increased oxygen vacancies. But at higher temperature, loss of oxygen will be increased with increasing Ni doping due to lower binding energy of Ni–O bond as compare to Mo–O bond. This will reverse the conductivity trend for the Ni doped samples which can be seen from the Fig. 4.8. It is also supported by the increasing nature of the activation energies of the Ni doped samples.

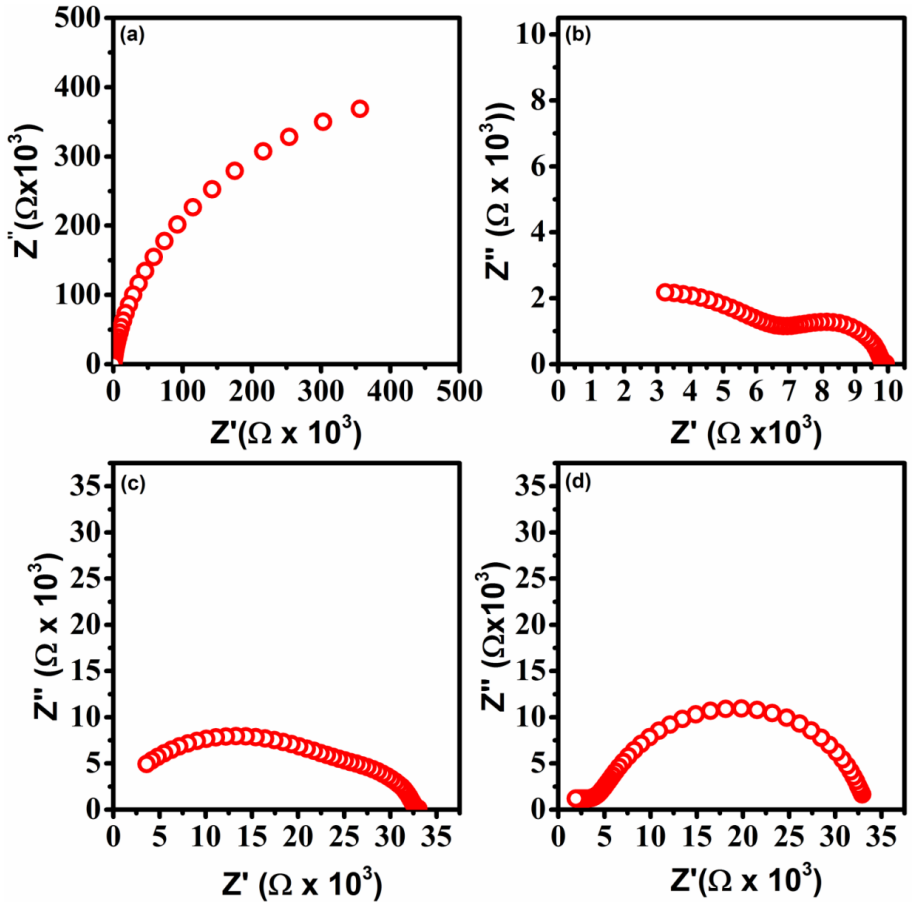

Fig. 4.7: *The complex plane Impedance plots for compositions* ***(a)*** *SNM00,* ***(b)*** *SNM05,* ***(c)*** *SNM10 and* ***(d)*** *SNM15 at 250 °C.*

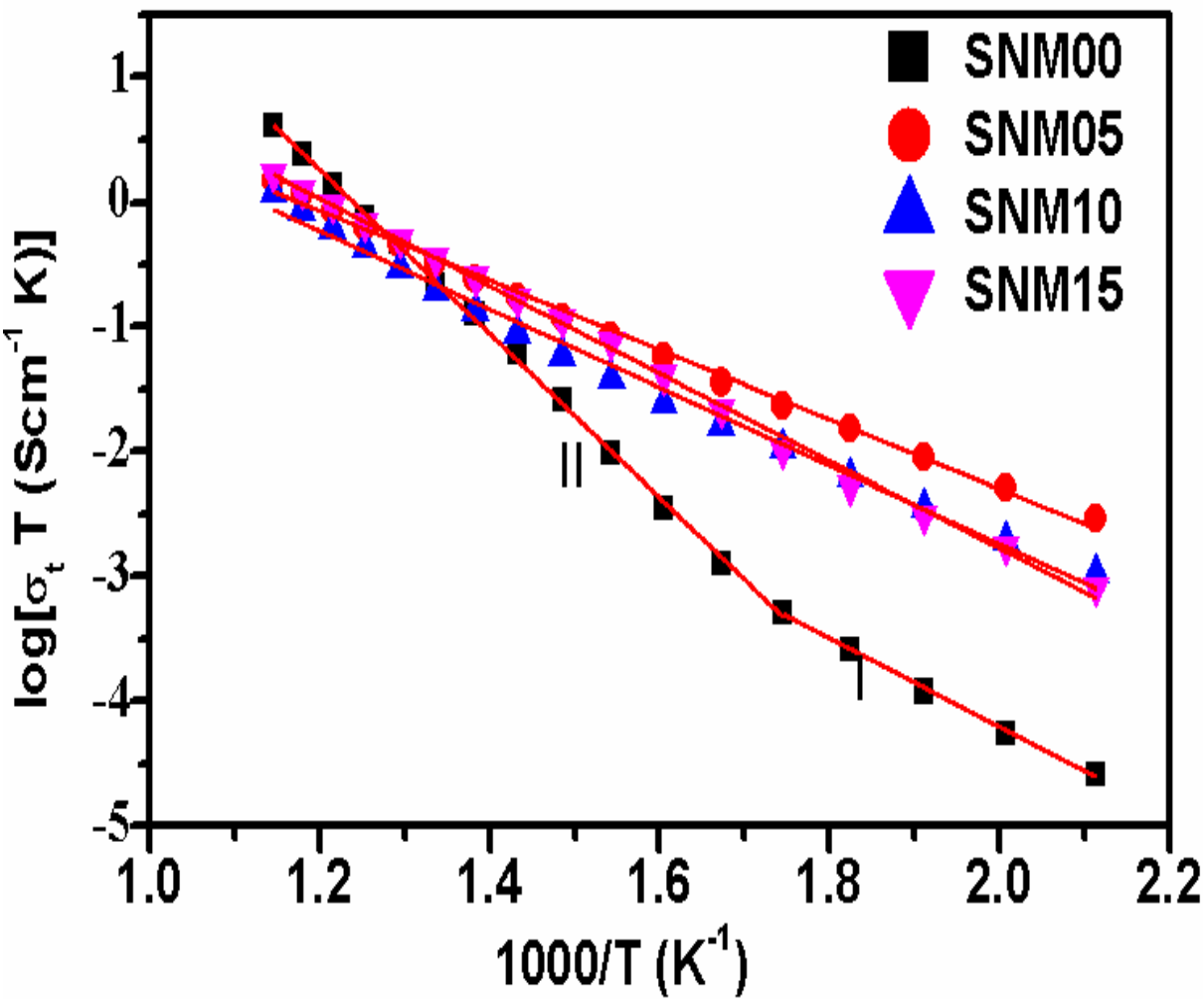

Fig. 4.8: *Arrhenius logσ_tT vs. 1000/T plots of various compositions of the system SNM-x (0.00 ≤ x ≤ 0.15).*

Table 4.4: *Activation energy of the system SNM-x (0.00 ≤ x ≤ 0.15).*

Compositions	Temperature Range	Activation energy, E_a (eV)
SNM00	200˚C - 300 ˚C 300˚C - 600 ˚C	0.66 1.24
SNM05	200˚C - 600 ˚C	0.57
SNM10	200˚C - 600 ˚C	0.57
SNM15	200˚C - 600 ˚C	0.64

4.3.6 Conductivity Measurement of Sr_2NiMoO_6 (SNM00) in Reducing Atmosphere

In the previous section, the electrical properties of the doped Sr_2NiMoO_6 system were discussed. It is considered worthwhile to measure electrical conductivity of the base composition, Sr_2NiMoO_6, in the reducing atmosphere. Figure.4.9 shows a plot of temperature dependant resistance for $Sr_2NiMoO_{6-\delta}$ (SNM00) system in reduced H_2 atmosphere, which was measured in temperature range of 100-700°C during the cooling cycle. This figure clearly reveals that resistance value decreases with increasing temperature and get almost constant value above 500 °C. Figure.4.10 shows the Arrhenius plots of the conductivity (σ) of $Sr_2NiMoO_{6-\delta}$ (SNM00) in H_2 as well as in air atmosphere in temperature range 200°C-600°C. The conductivity in reduced atmosphere is highly applicable as potential SOFC anode materials.

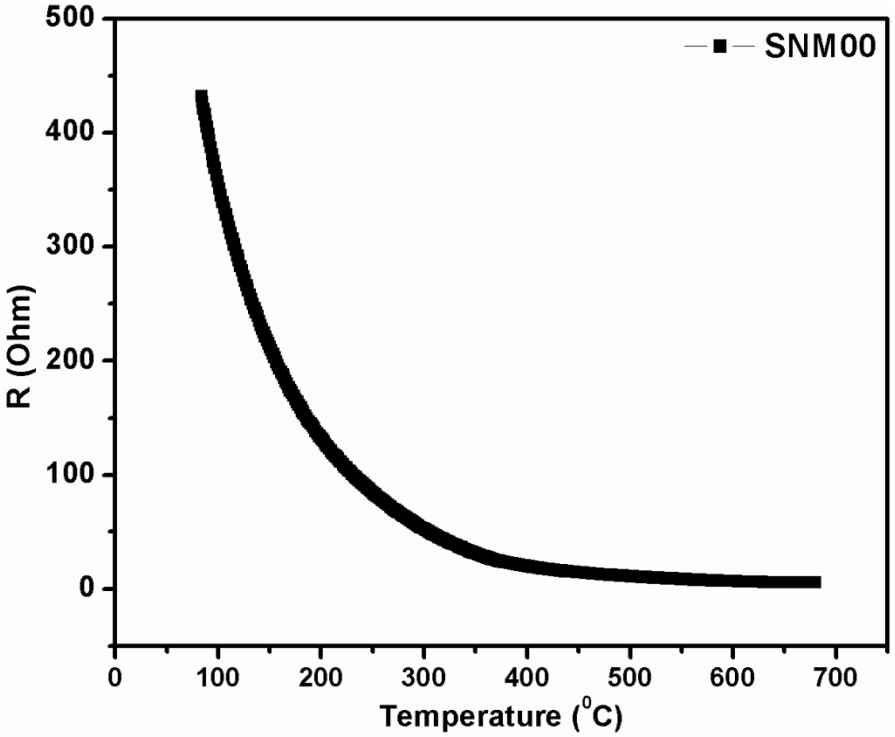

Fig.4.9: *The plots of Resistances (R) vs. Temperature for the $Sr_2NiMoO_{6-\delta}$ (SNM00) sample in H_2 atmosphere.*

In H_2 atmosphere, sample SNM00 exhibits small polaron hopping conduction mechanism [Wei et al. (2008)]. The value of conductivity depends on the reduced state of the sample. Before reduction (in Air) sample showed the low conductivity after that the

conductivity increases to a great extent, because reduction in H_2 leads to the formation of oxygen vacancies in the double-perovskite structure [Wei et al. (2008)]. Formation of more oxygen vacancies reduces Mo^{6+} to Mo^{5+} which attributes to an increase in the concentrations of both Mo^{5+} ions and small polarons.

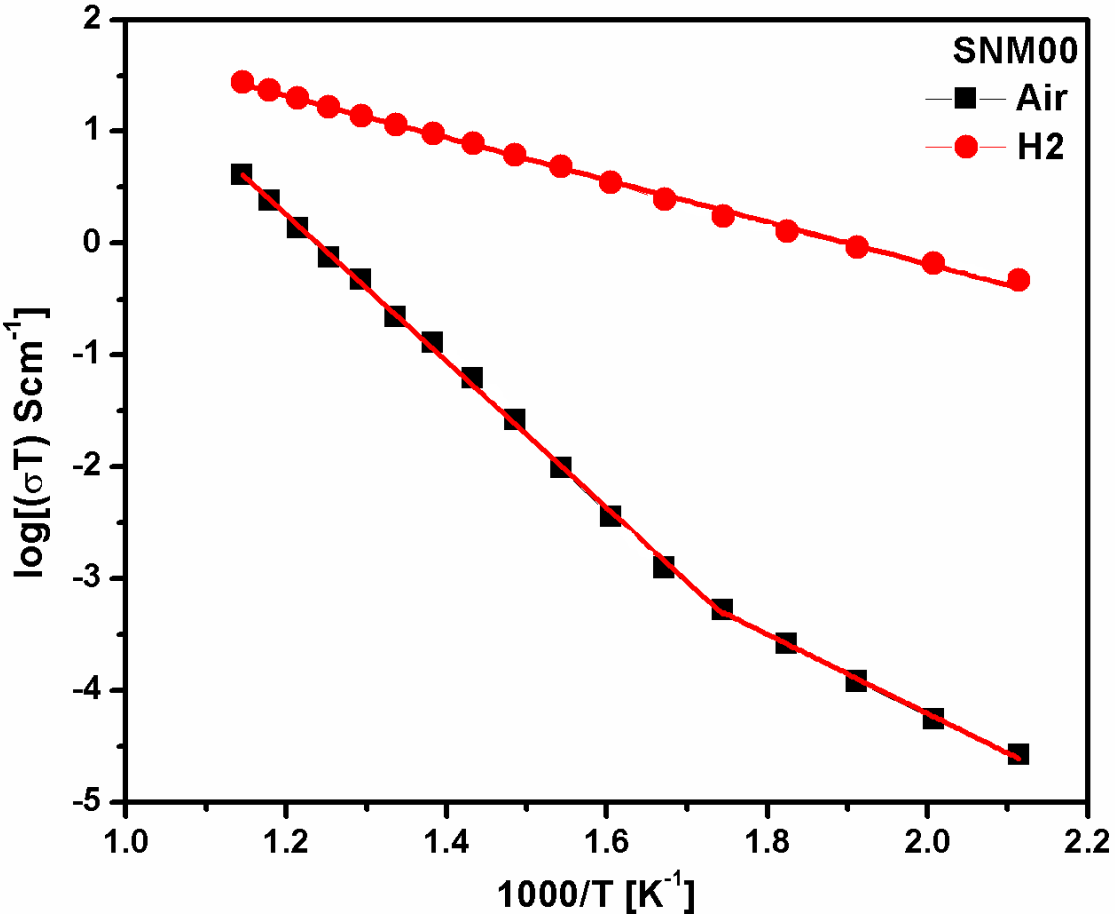

Fig.4.10: *Arrhenius plots of conductivity for the $Sr_2NiMoO_{6-\delta}$ (SNM00) sample in H_2 and air atmosphere.*

The enhanced small polarons lead to a relatively high conductivity and excellent mixed electronic- ionic conductivities. The value of the electrical conductivity of SNM00 in H_2 atmosphere at ~700 °C is found to be 0.054 S/cm. [Huang et al. (2006) and Ullmann et al. (2000)]. Huang et al. (2009) reported that the electrical conductivity value of $Sr_2NiMoO_{6-\delta}$ system exhibit ~1.11 Scm^{-1} in reduced atmosphere at 800 °C. Vasala et al. [2010] also reported that the formation of more oxygen-vacancy concentration should be a positive factor regarding the SOFC-anode performance. The activation energy value is obtained from the slopes of the Arrhenius plots of log (σT) vs. 1000/T is found 0.37 eV in H_2. The value of

activation energy in H_2 also exhibits as lower than observed in air. Figure 4.10 also reveals that a reducing atmosphere suppresses the phase transition observed in SNM00 at 300 °C.

4.4 Conclusions

Double perovskite materials in the system $Sr_2Ni_{1+x}Mo_{1-x}O_{6-\delta}$ were prepared by a facile solution combustion technique. All the samples exhibit tetragonal structure with space group I4/m. The average TEC values for the system SNM-x found to be compatible to standard electrolyte materials YSZ and LSGM. XPS spectra show the decreasing concentration of charge carriers $\left[Mo_{Mo^{6+}}^{5+}{}'\right]$ on increasing Ni doping, which is mainly responsible for conduction at lower temperature. XPS spectra also reveal that the Ni at Mo site probably exist in Ni^{3+} state. With increasing Ni content, oxygen vacancies increases for sample SNM05 and afterward decreases for samples SNM10 and SNM15, while at higher temperature contribution of oxide ions to the conductivity increase with increasing Ni content due to weaker bond of Ni–O as compared to Mo–O bond, which facilitate the release of oxygen and hence reverse the conductivity trend for the Ni doped samples. In the prepared samples, SNM05 has better electronic conductivity and hence it may act as a potential anode candidate in solid oxide fuel cells. As for practical application of Sr_2NiMoO_6 materials in SOFC, the study on stability of phases as well as conductivity in reducing atmosphere is found better performance than that of air.